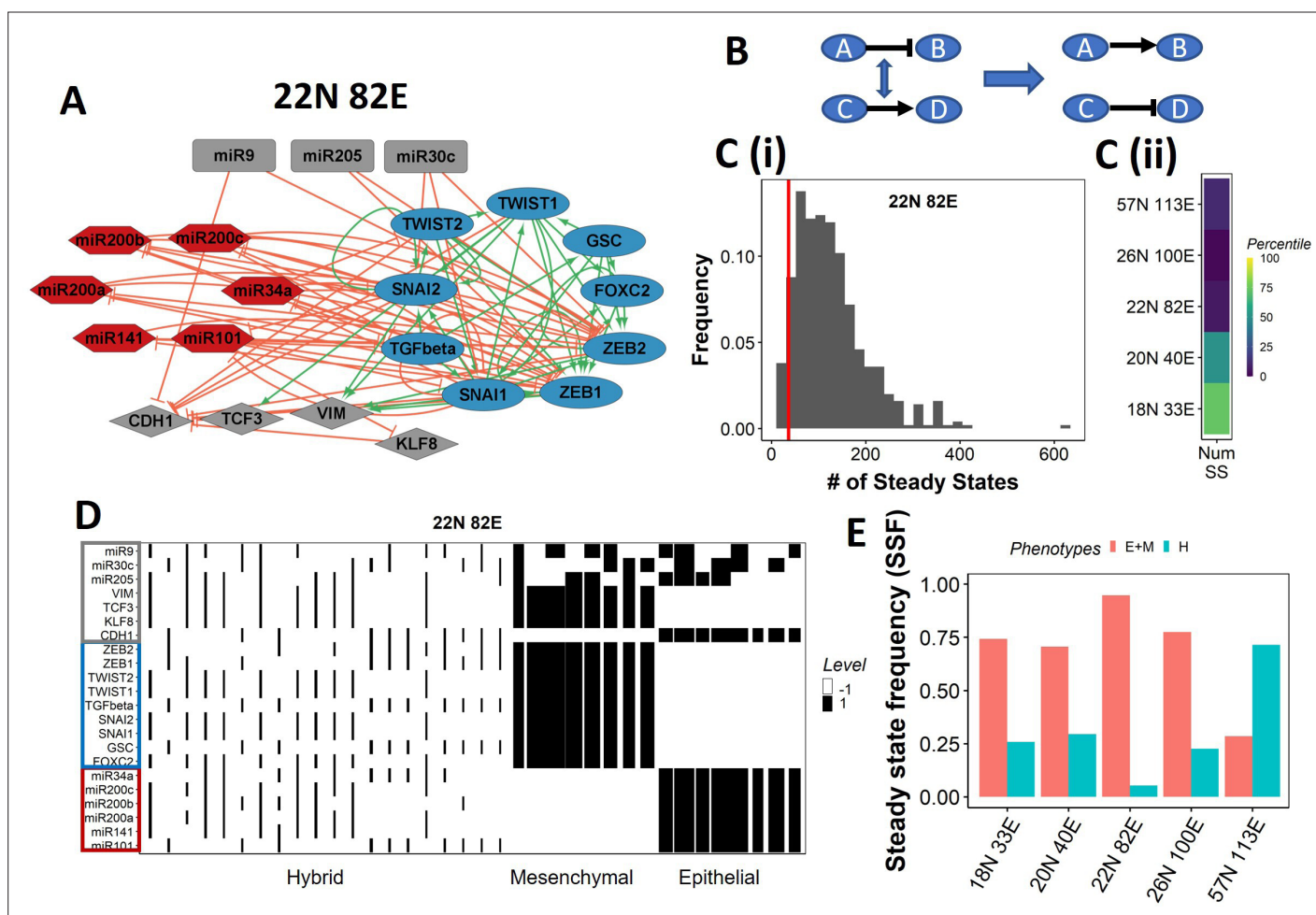


---

## Figures and figure supplements

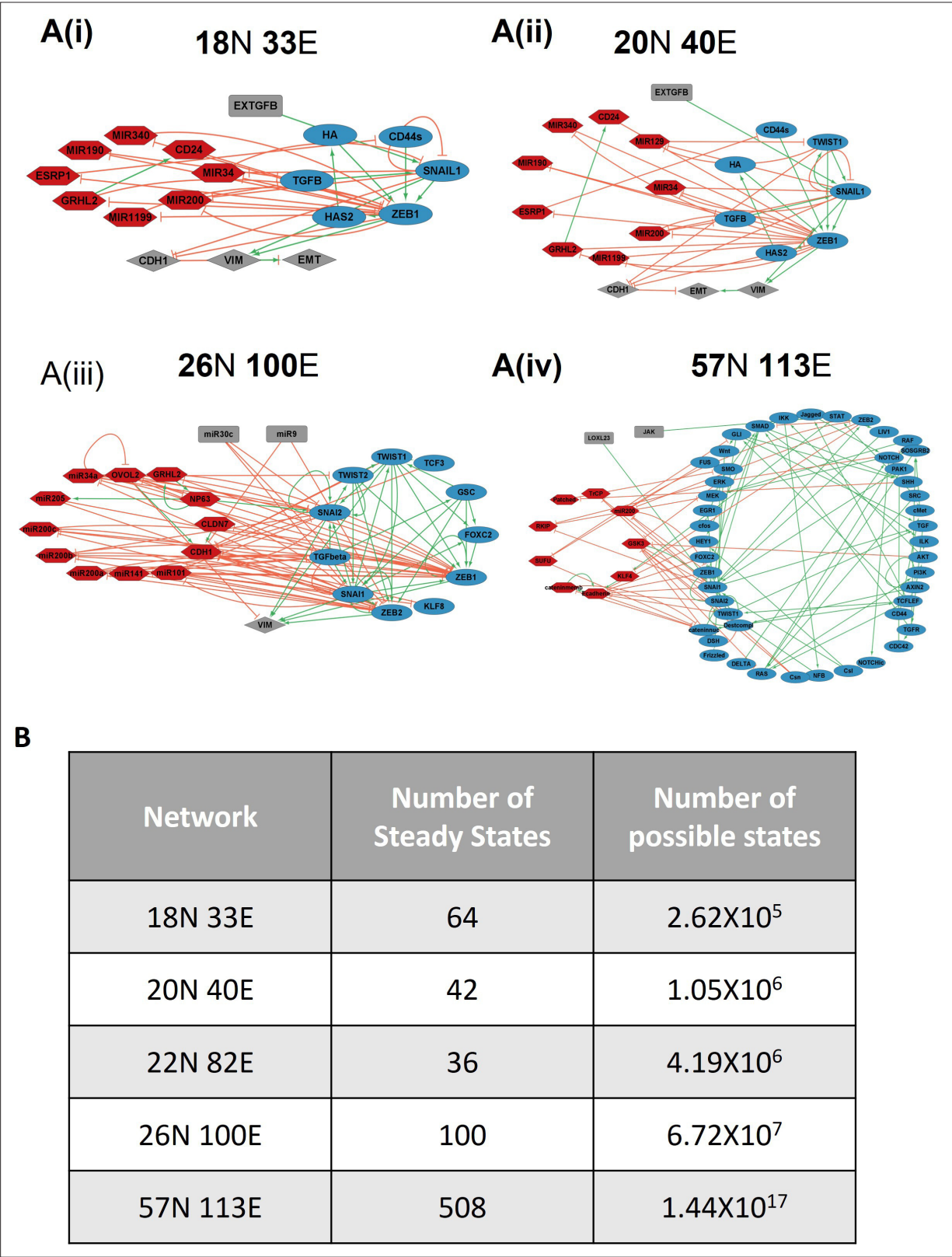
Landscape of Epithelial Mesenchymal Plasticity as an emergent property of coordinated teams in regulatory networks

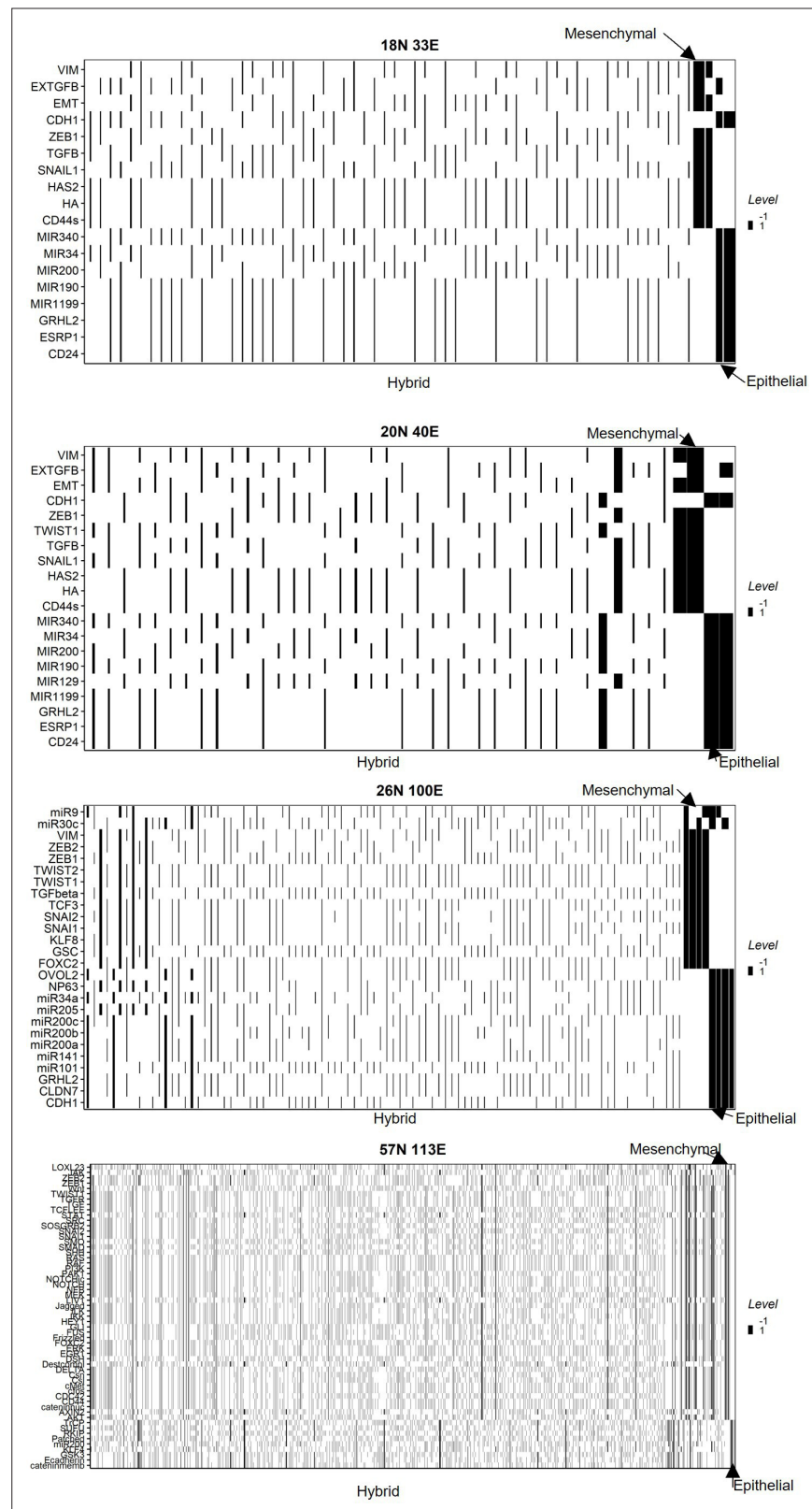
**Kishore Hari *et al***



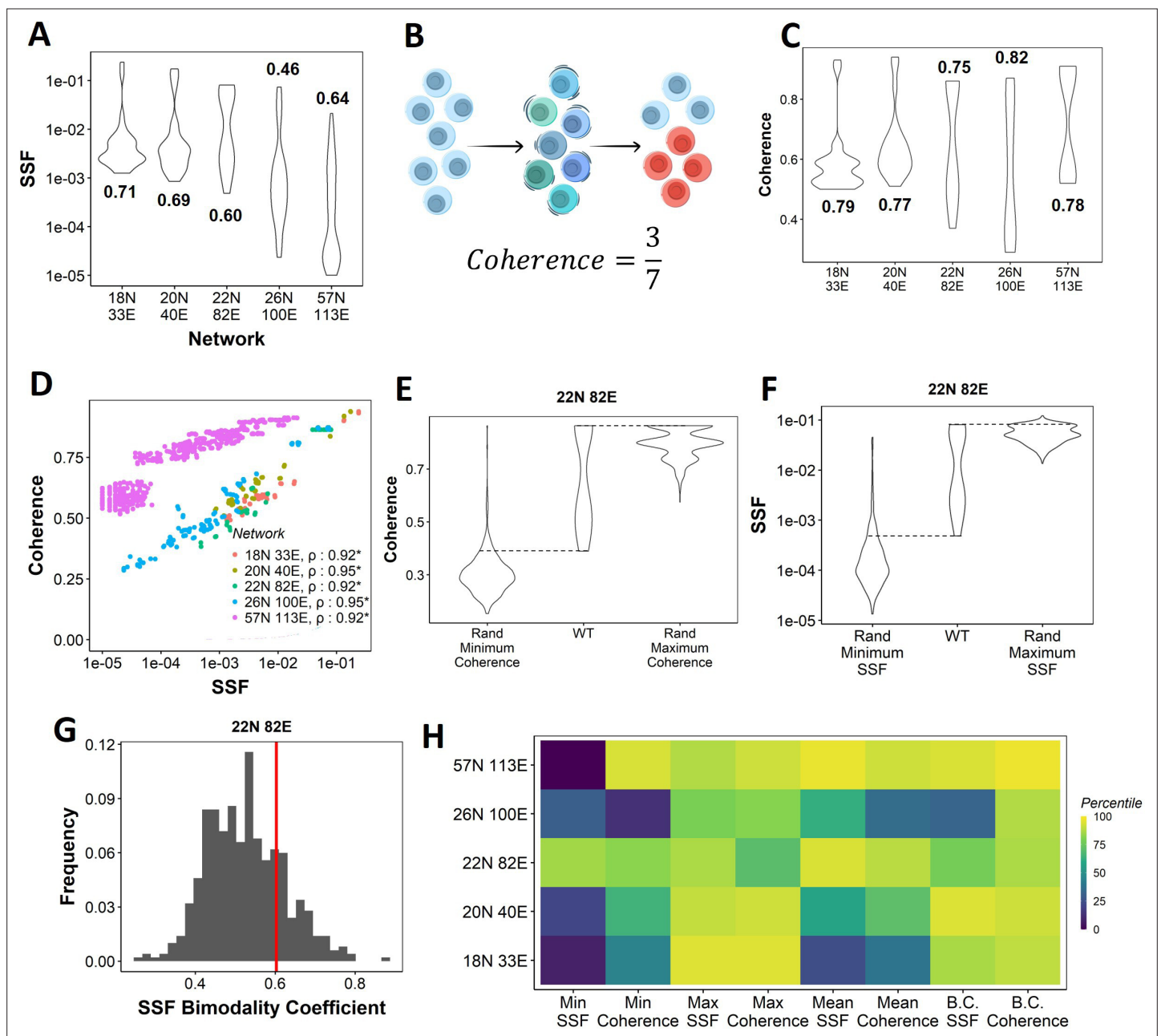
**Figure 1.** EMP network topology can result in a bimodal phenotypic stability landscape. **(A)** EMP network of size 22 N 82E, where N stands for number of nodes and E stands for number of edges. **(B)** Demonstration of network randomization **(C)** (i) Distribution of number of steady states in random networks of size 22 N 82E. The wild-type EMP network of the same size is represented using the red line. (ii) Percentile of the WT network in the distribution of the number of steady states in random networks. **(D)** Heatmap depicting the steady states of the 22 N 82E network. Each column represents a steady state. Each row represents a node. White cells indicate low expressing/inactive node (-1) in a state and black cells indicate high expression/active (1). The width of each column is proportional to the frequency of the given steady state. **(E)** Comparison of the cumulative frequency of the terminal (Epithelial and Mesenchymal) states vs that of the hybrid states for all five EMP networks.



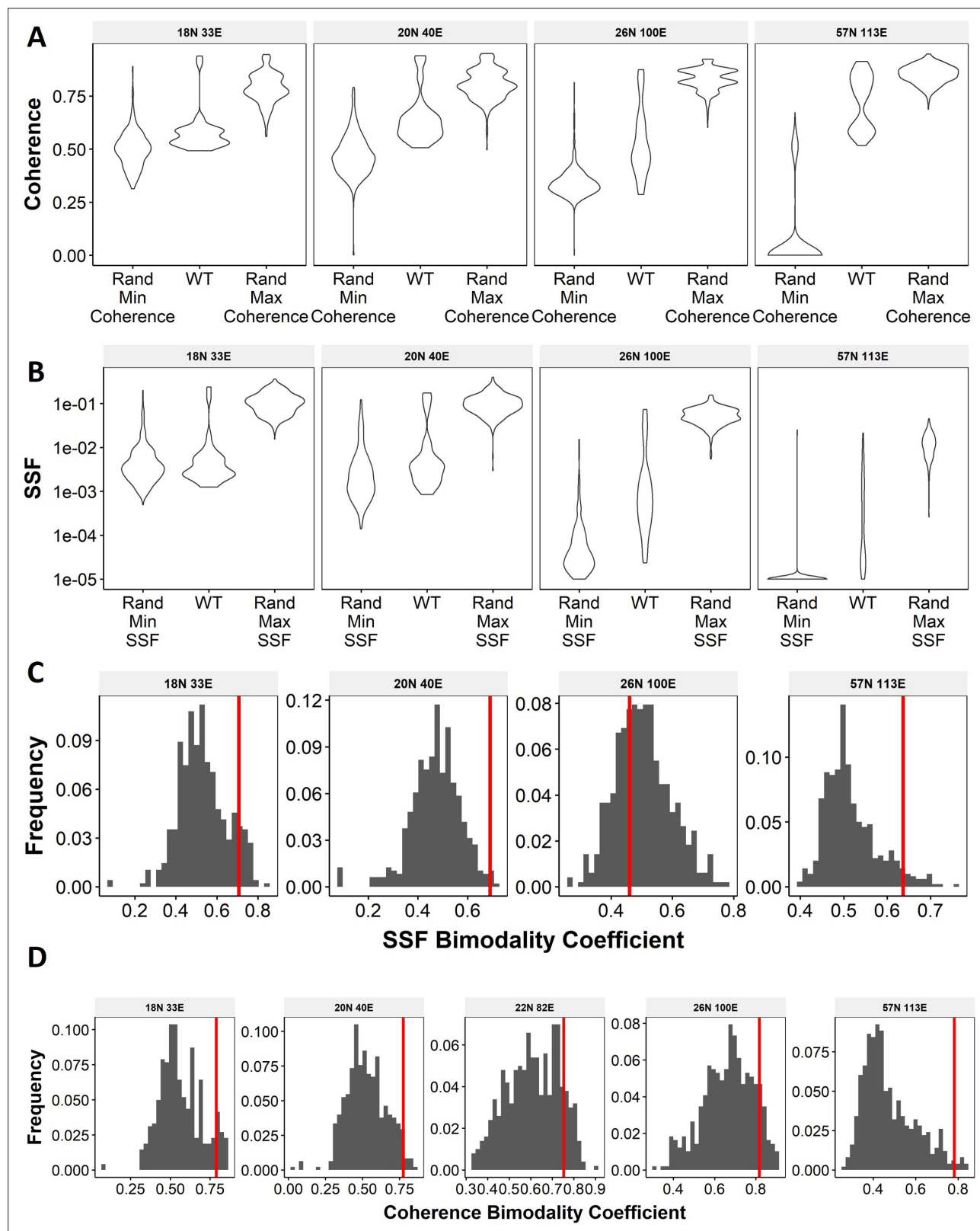




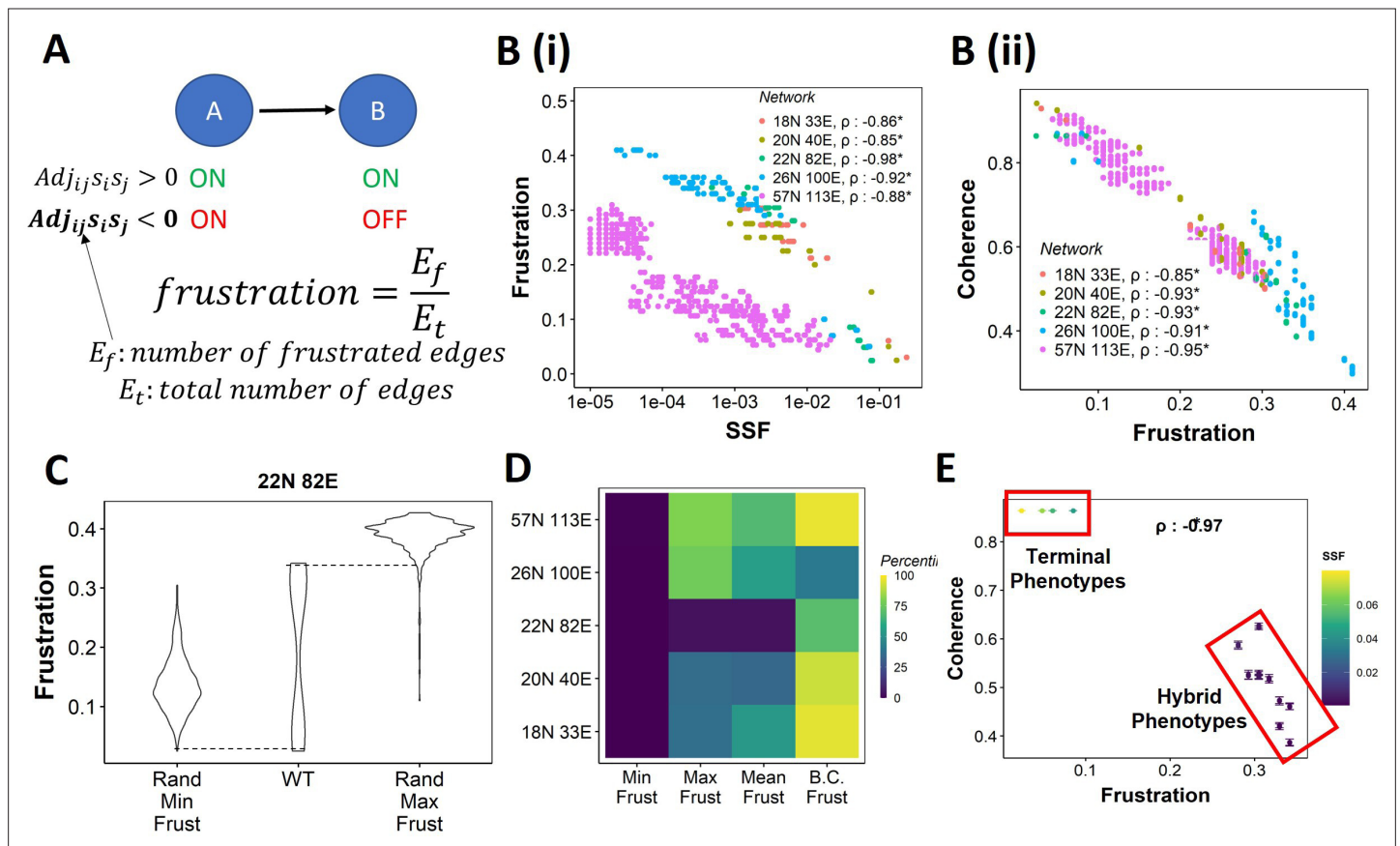
**Figure 1—figure supplement 2.** Heatmaps depicting the steady states of the EMP networks. Each row represents the activity of a node (−1 or 1), and each column represents a steady state.



**Figure 2.** Dynamical traits of phenotypes observed from WT EMP networks and their randomised counterparts. **(A)** Distribution of Steady state frequency (SSF) of the steady states obtained for the five EMP networks, in log10 scale. The corresponding Sarle's bimodality coefficients have been reported. A value greater than 0.55 indicates bimodality. **(B)** Depiction of coherence calculation. The blue balls indicate unperturbed steady state (P1, say). The green and dark blue balls represent the perturbations given to the steady state. The red balls represent a different steady state that the system reached after the perturbation. The fraction of perturbations that reverted to the original state P1 (3 out of 7 balls) is calculated as coherence. **(C)** Similar to A, but for coherence of the steady states of WT EMP Networks. **(D)** Scatterplot between coherence and SSF of WT EMP networks. Spearman correlation coefficient for each network has been reported. \*:  $p < 0.05$ . **(E)** Comparison of the distribution of coherence of the steady states of WT EMP network (22 N 82E), with the distribution of maximum coherence values and minimum coherence values of the corresponding random networks. **(F)** Similar to E, but for SSF. **(G)** Distribution of the SSF bimodality coefficients for random networks of size 22 N 82E. The red vertical line represents the WT network. **(H)** Percentile of the WT networks in the distribution of multiple stability metrics obtained from random networks.

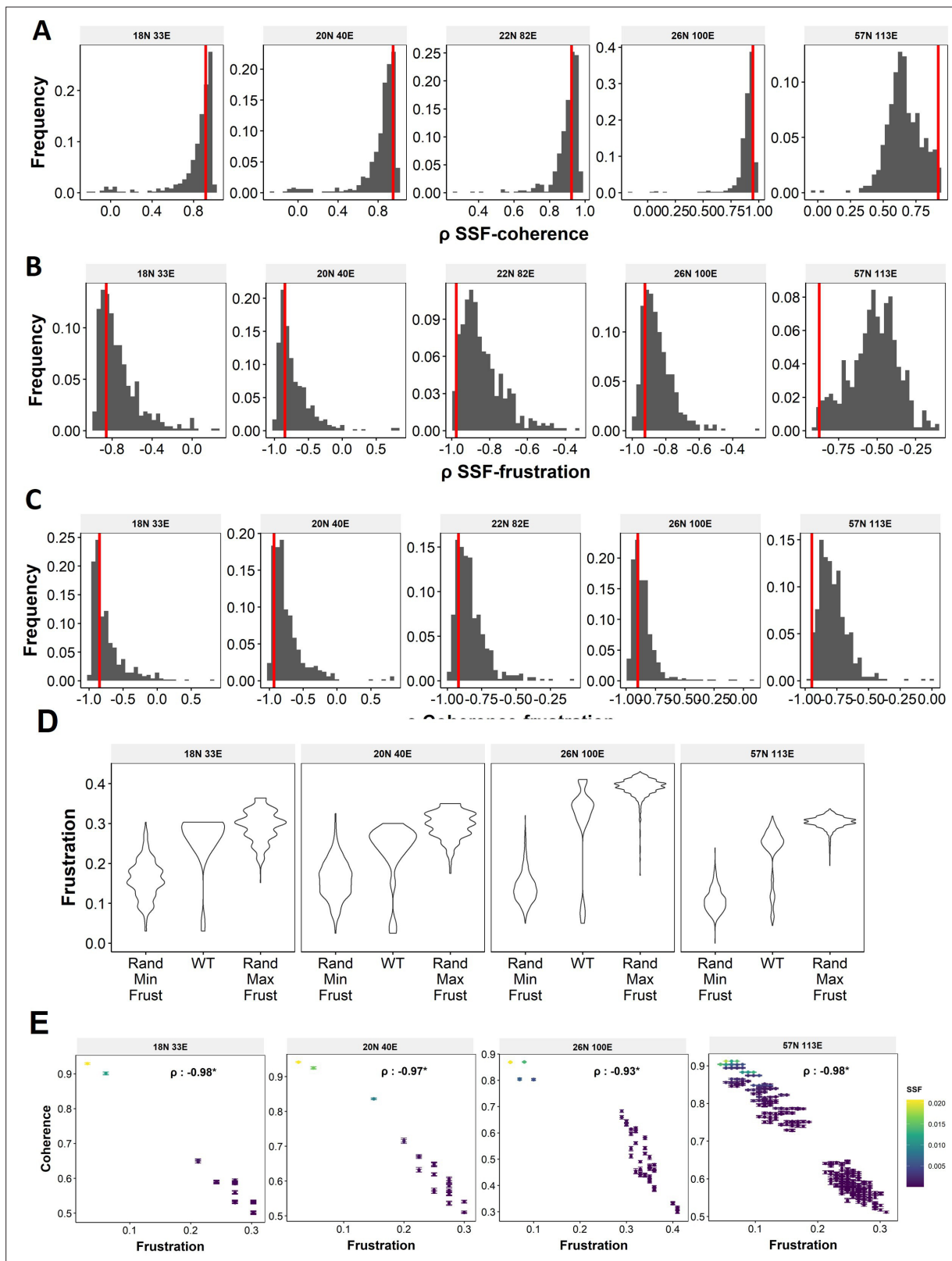


**Figure 2—figure supplement 1.** (A) Comparison of the distribution of SSF of the steady states of WT EMP networks with the distribution of maximum SSF values and minimum SSF values of the corresponding random networks. (B) Same as (A) but for coherence (C) Distribution of the SSF bimodality coefficients for random networks corresponding to WT EMP networks. The corresponding WT network in each panel is represented by the red vertical line. D Same as C but for coherence.

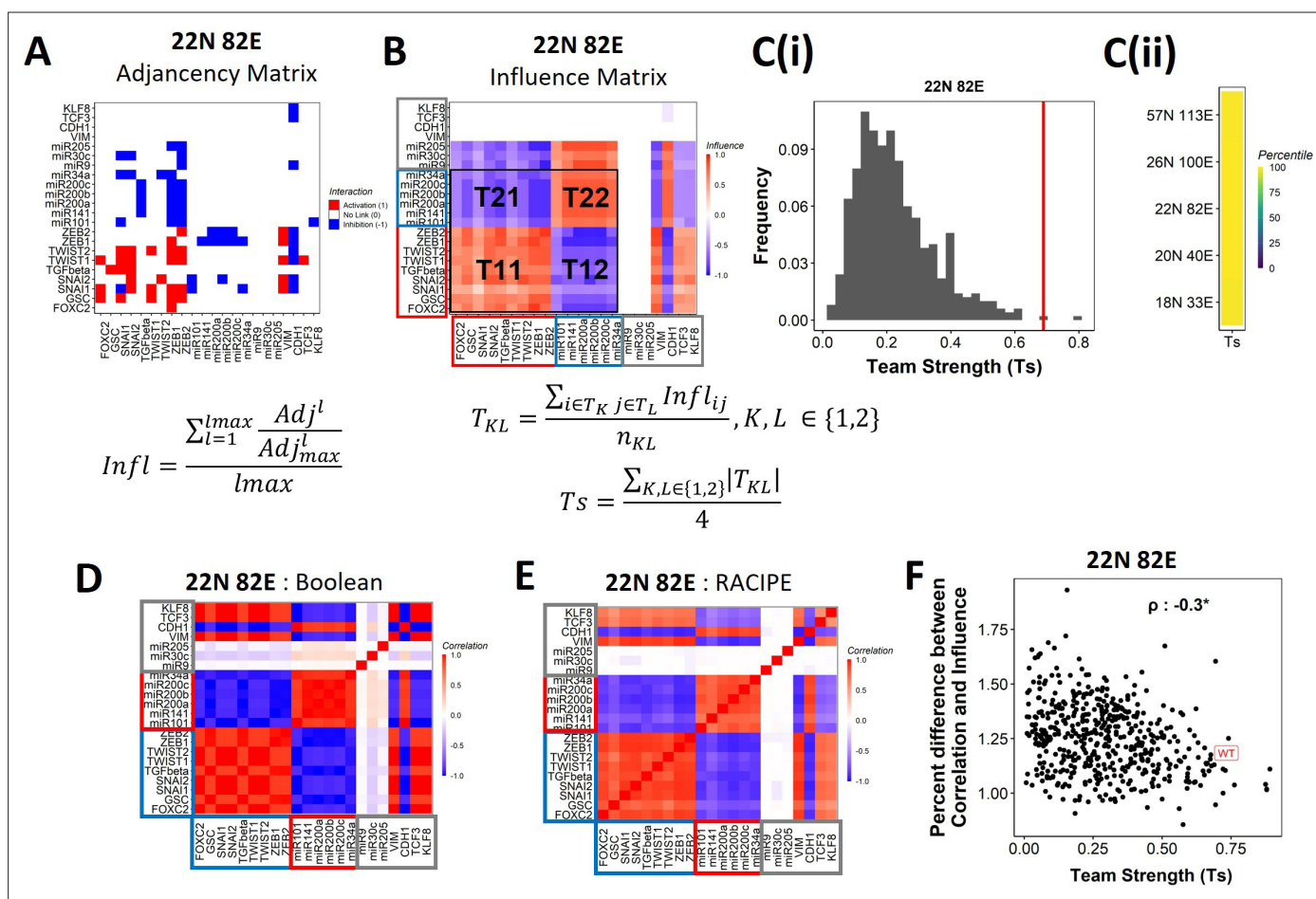


**Figure 3.** Frustration as a stability metric for WT and random networks. **(A)** Depiction of calculation of frustration. represents the interaction from  $i^{th}$  node to  $j^{th}$  node,  $s_i$  and  $s_j$  represent the activity of the  $i^{th}$  node and the  $j^{th}$  node for a given state  $S$ . **(B)** Scatterplot between Frustration and (i) SSF, (ii) Coherence for WT EMP networks.. Spearman correlation coefficient for each network has been reported. \*:  $p < 0.05$ . Each dot corresponds to a steady state for the given network. **C** Comparison of the distribution of frustration of the steady states of WT EMP network (22 N 82E), with the distribution of maximum frustration values and minimum frustration values of the corresponding random networks. **(D)** Heatmap of the percentile of WT network values in the random network value distribution for the minimum, maximum and mean frustration. **(E)** Representation of WT steady states in a scatterplot of frustration and coherence with the color representing the corresponding SSF. Spearman correlation coefficient between the axis metrics is reported. \*:  $p < 0.05$ . The terminal and hybrid phenotypes are highlighted with red rectangles.

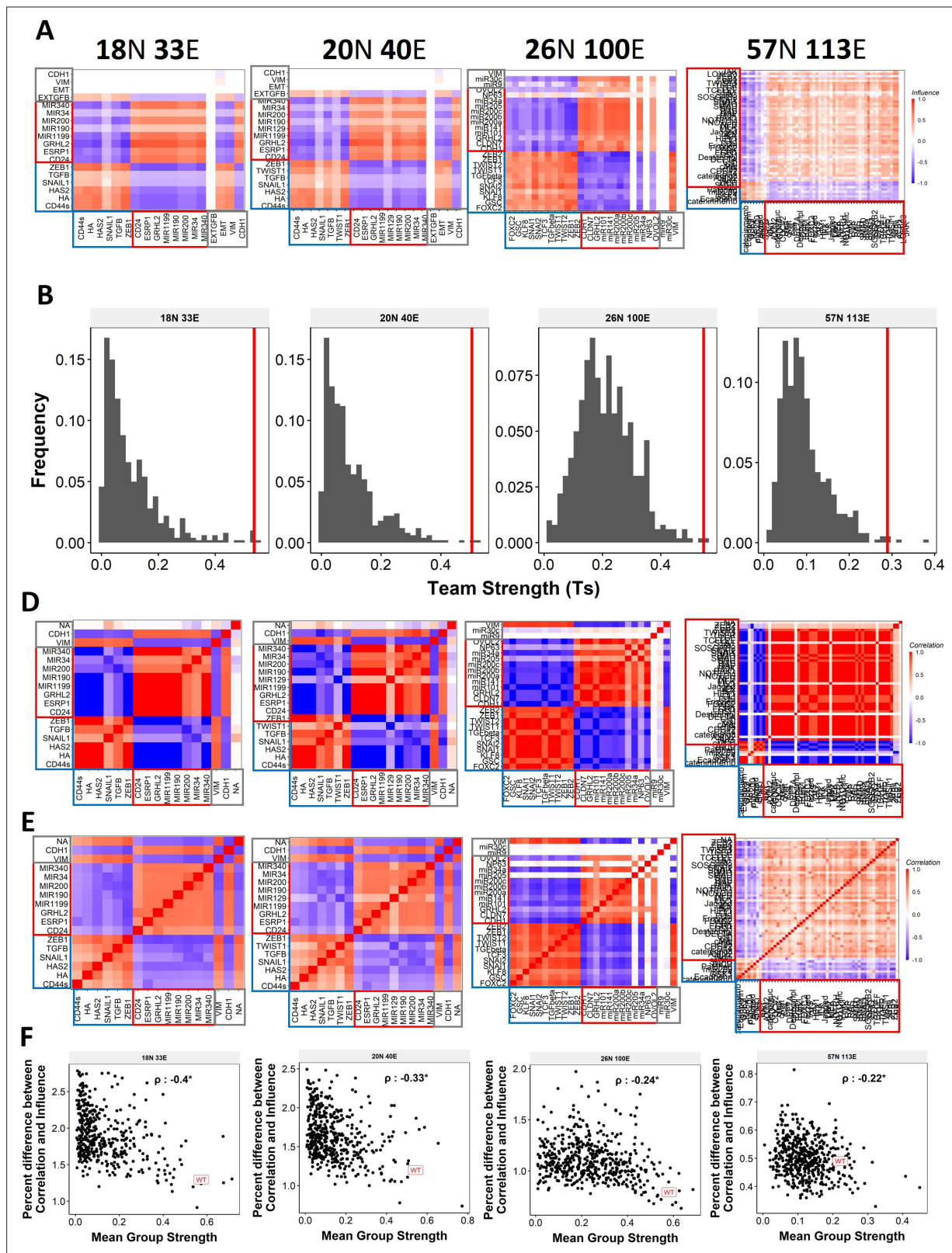




**Figure 3—figure supplement 1.** (A–C) Distribution of spearman correlation coefficient of (A) SSF – coherence, (B) SSF-Frustration and (C) Coherence – Frustration for random networks corresponding to WT EMP networks. The corresponding WT network in each panel is represented by the red vertical line D Comparison of the distribution of Frustration of the steady states of WT EMP networks with the distribution of maximum Frustration values and minimum Frustration values of the corresponding random networks. E Representation of WT steady states in a 2-d stability axes with color as SSF.



**Figure 4.** EMP networks consist of two well-coordinated teams. **(A)** Adjacency matrix of the 22 N 82E network. Each row depicts the links originating from the node (i.e., input) corresponding to the row (y axis) and all other nodes (x axis, outputs). The color represents the nature of the edge: red for activating links, blue for inhibiting links and white for no links. The formula for the conversion of adjacency matrix to influence matrix is given below the panel, where  $Adj$  is the adjacency matrix,  $Adj_{max}$  is the adjacency matrix with all  $-1$ 's replaced with  $1$ 's.  $Adj^l$  is the adjacency matrix raised to the power of  $l$ . The division  $\frac{Adj^l}{Adj_{max}^l}$  is element-wise.  $l_{max}$  is the maximum path-length considered for calculating the influence. **(B)** The influence matrix for the 22 N 82E network. The signal and output nodes (peripheral) are highlighted with a grey box, the mesenchymal nodes (team 1) are highlighted with a blue box and the epithelial nodes (team 2) are highlighted with a red box. The formula for team strength ( $T_s$ ) is given below the influence matrix.  $T_1$  and  $T_2$  represent the two teams of nodes in the network (Epithelial and Mesenchymal nodes respectively).  $n_{KL}$  is the number of cells in the rectangle  $T_{KL}$ . **(C)** (i) Distribution of team strength ( $T_s$ ) for random networks of size 22 N 82E. The  $T_s$  value for the corresponding wild-type EMP network has been highlighted using the red vertical line. (ii) Percentiles corresponding to the WT team strength in the corresponding distribution obtained from random networks for networks of all sizes (y-axis). **(D)** Correlation matrix for the expression levels of nodes of the 22 N 82E network, as obtained by the Boolean formalism. **(E)** Same as D but for RACIPE. **(F)** Scatterplot of the difference between the influence matrix and Boolean correlation matrix (y-axis) and the mean group strength of the network (x-axis) for random networks of size 22 N 82E. The wild-type EMP network is highlighted in red. Spearman's correlation coefficient is reported. \*:  $p < 0.05$ .



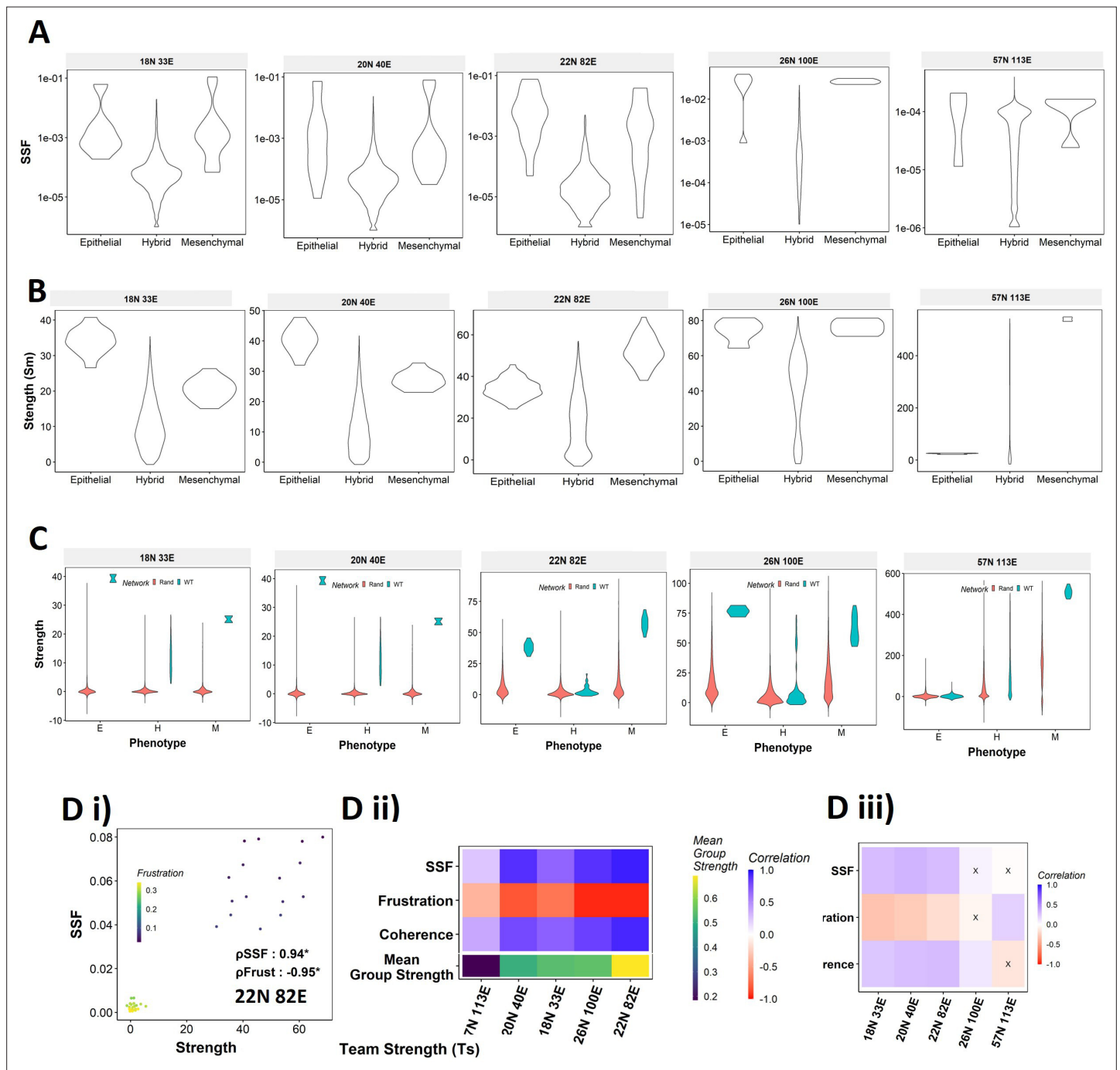
**Figure 4—figure supplement 1.** (A) Distribution of SSF for the RACIP states of 22 N 82E WT EMP network. The state classification is done based on teams identified in B. (B) Distribution of the strength of states of the EMP networks from RACIP (C) Comparison of the state strength distributions for Epithelial, Mesenchymal and Hybrid phenotypes obtained from WT and random networks of labelled sizes. (D) (i) Correlation of state strength with SSF and Frustration for 22 N 82E WT network. (ii) Correlation between the stability metrics (y axis) and the strength for the states of the five different WT

Figure 4—figure supplement 1 continued on next page

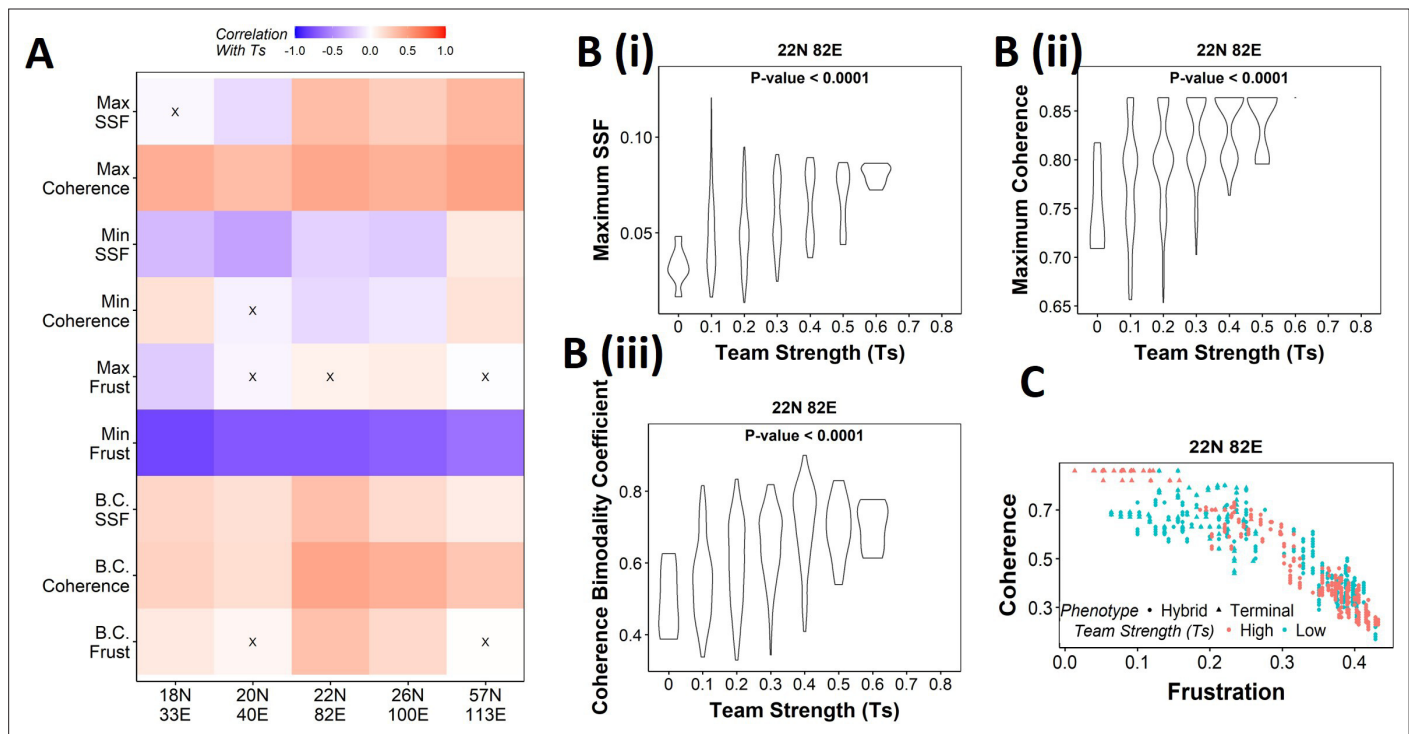


Figure 4—figure supplement 1 continued

EMP networks (x-axis). The team strengths of the networks is represented using a different color scheme at the bottom of the heatmap. (iii) Correlation between the quantities in E(ii) and Gs for random networks of corresponding to WT networks of different sizes  $X$  :  $p > 0.05$ .



**Figure 4—figure supplement 2.** (A) Influence matrices for the EMP networks. (B) Distribution of the team strength (Ts) for EMP networks (i) 18 N 33E, (ii) 20 N 40E and (iii) 26 N 100E. (C) Correlation matrices for Boolean expression levels of EMP networks, in increasing order of number of nodes except for 22 N 82E network. (D) Same as C but for RACIPE. (E) Similar to **Figure 2F**, for networks other than 22 N 82E.



**Figure 5.** Strong teams support the bimodal EMP landscape. **(A)** Heatmap depicting the spearman correlation of Ts with stability metrics and frustration metrics for random networks of all sizes (y-axis). Insignificant correlations ( $p > 0.05$ ) are marked by "X". **(B)** Violin plots depicting the effect of change in Ts against the maximum stability metrics (i) Maximum SSF (ii) Maximum coherence and (iii) Coherence Bimodality Coefficient for random networks of size 22 N 82E. The p value for 1-way ANOVA is reported. **(C)** Scatter plot showing the states of top 10 and bottom 10 (based on mean group strength) random networks of size 22 N 82E.

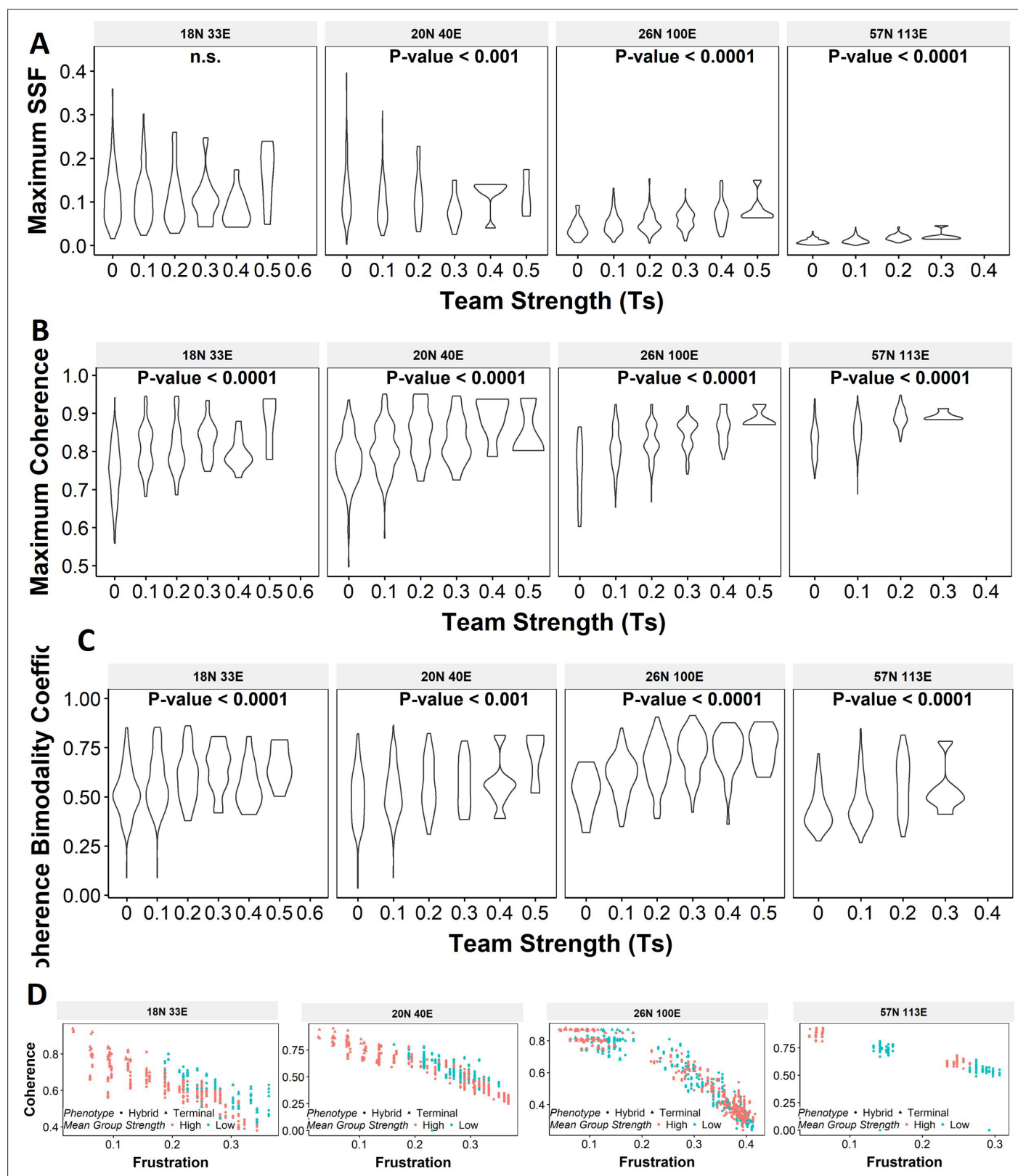


**Figure 5—figure supplement 1.** (A–C) Violin plots depicting the effect of change in Ts against the maximum stability metrics (A) Maximum SSF (B) Maximum coherence and (C) Coherence Bimodality Coefficient for random networks of size 22 N 82E. The p value for 1-way anova is reported. (D) Scatter plot showing the states of top 10 and bottom 10 (based on mean group strength) random networks of corresponding sizes labelled.

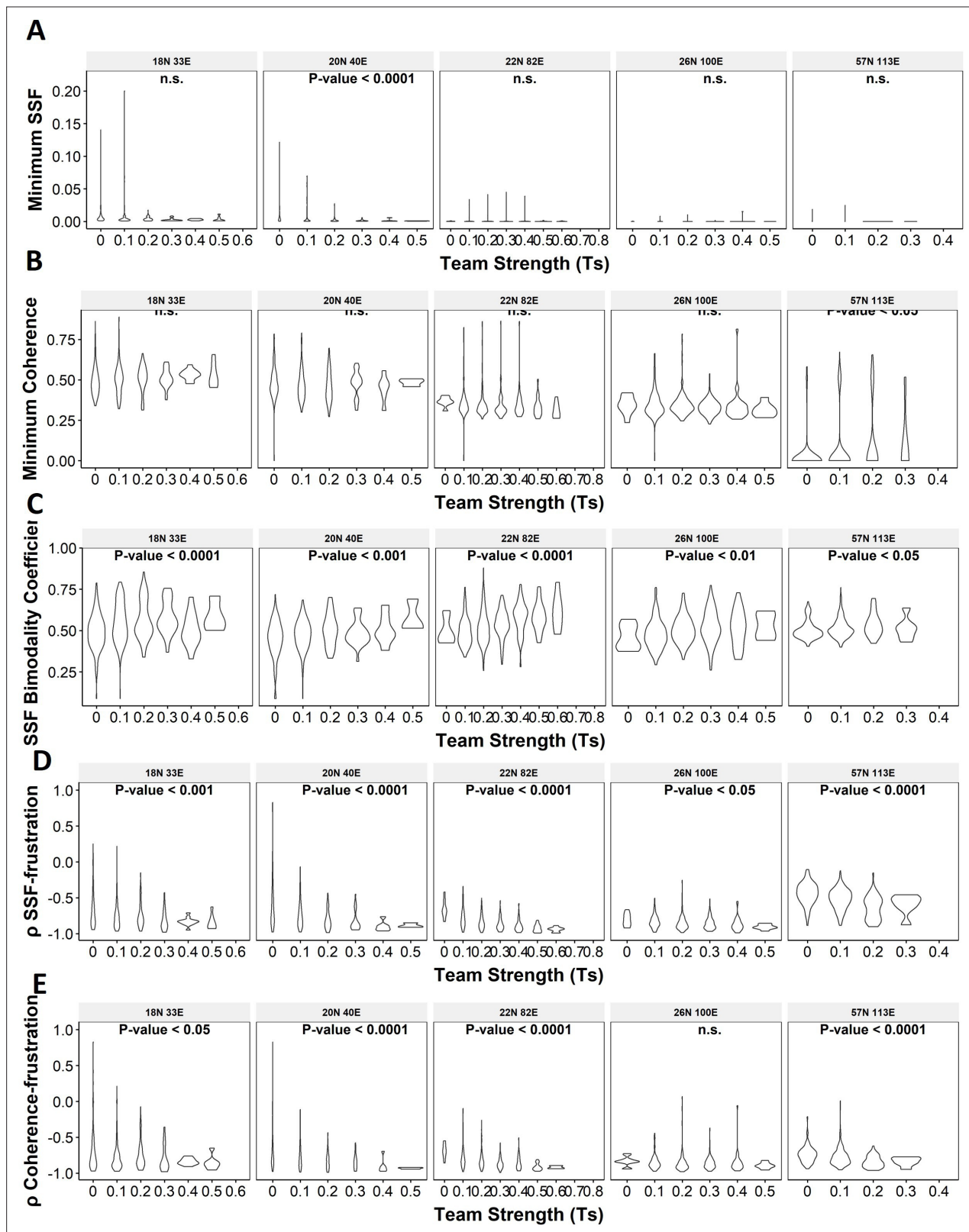


**Figure 5—figure supplement 2.** (A–C) Violin plots depicting the effect of change in Ts against the maximum stability metrics (A) Minimum SSF (B) Minimum coherence and (C) SSF Bimodality Coefficient (D–F Same as A–C but for Spearman correlation between (D) SSF-Frustration, (E) Coherence – Frustration and (F) SSF-Coherence.

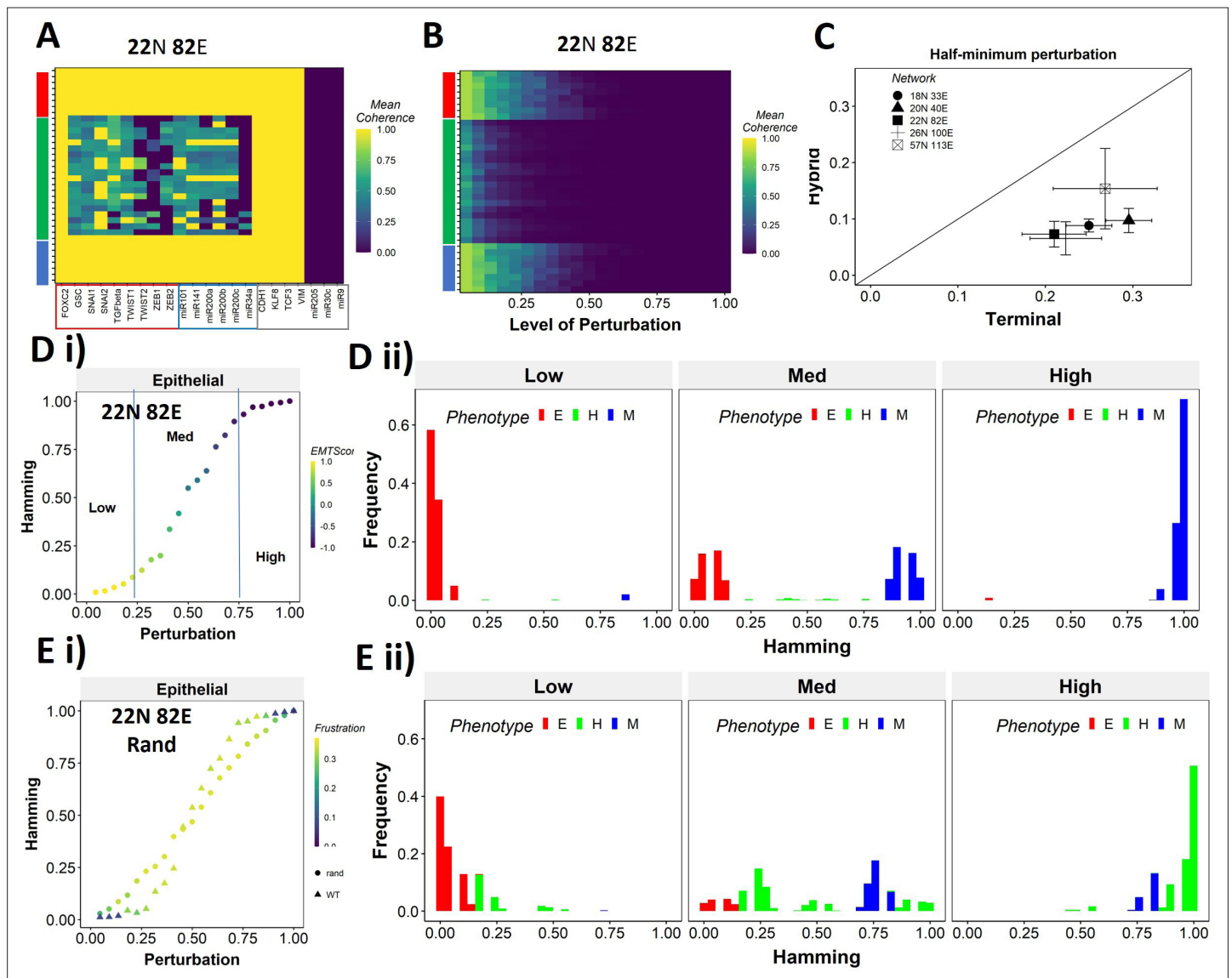


**Figure 6.** Teams of nodes impart distinct dynamical properties to terminal and hybrid phenotypes. **(A)** Heatmap depicting the mean coherence of the Boolean states of 22 N 82E WT EMP network when each node is individually perturbed. **(B)** Mean coherence of states of 22 N 82E EMP network with multiple nodes perturbed at once (Level of perturbation). **(C)** The extent of perturbation required to bring the coherence of terminal phenotypes (x-axis) and hybrid phenotypes (y-axis) below 0.5.  $x=y$  line is shown. **(D)** (i) Representative mean Hamming distance plot of an epithelial state obtained from 22 N 82E WT network. Three levels of perturbation are highlighted based on regions of the sigmoidal plot. (ii) Distribution of the Hamming distance from the starting state in D (i) at different levels of perturbation, colored by the phenotype. **(E)** (i) Representative mean Hamming distance plot comparing the dynamic transition of an epithelial state from WT and that from a random network. (ii) Corresponding distribution of Hamming distances for the random network.



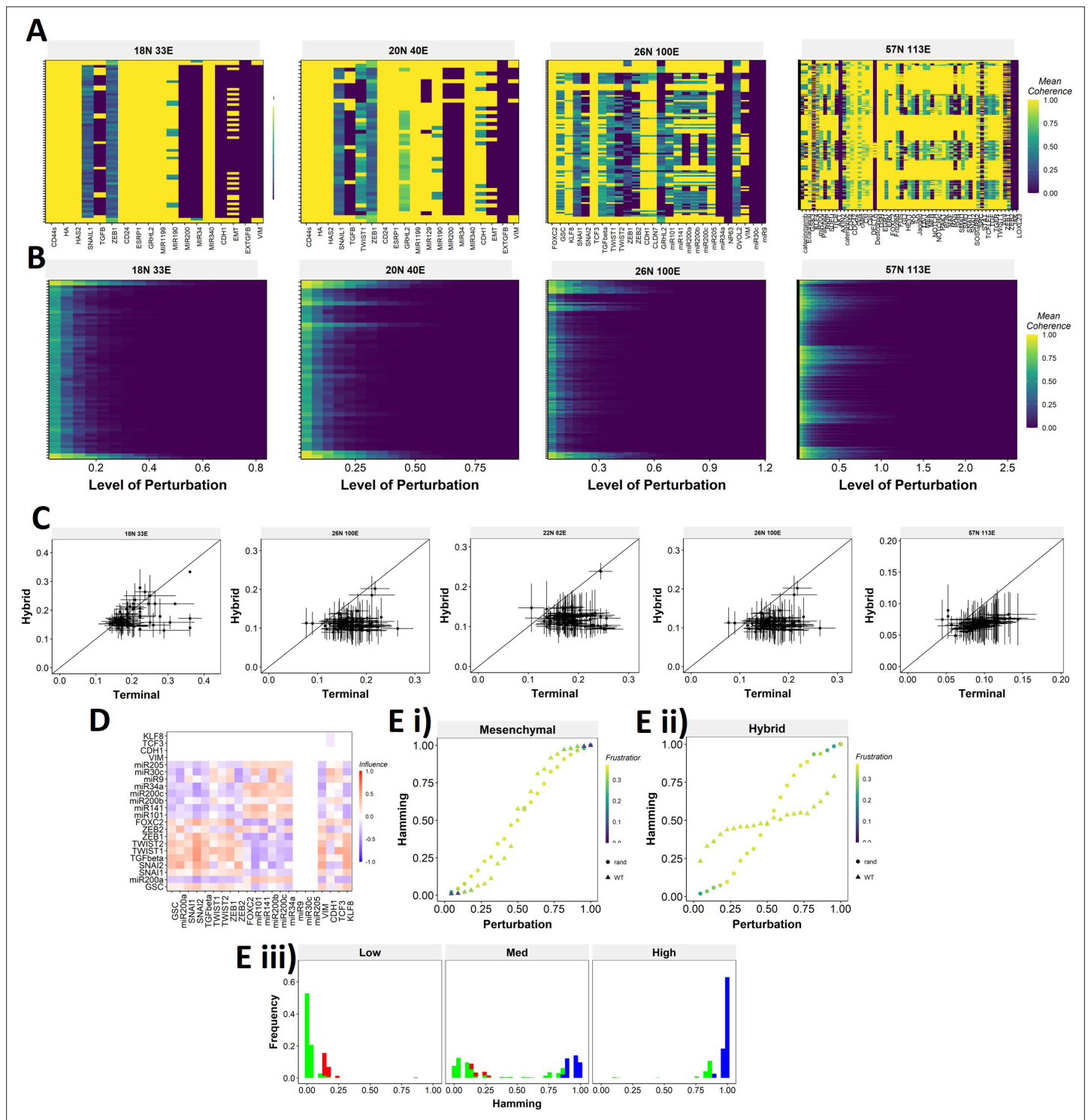


**Figure 6—figure supplement 1.** (A) Single node perturbation coherence heatmaps for WT EMP networks (B) Multi node perturbation coherence heatmaps for WT EMP networks (C) Half-minimum perturbation for terminal and hybrid states for the random networks. Each dot represents mean half-minimum perturbation for terminal and hybrid states for a network, and the bars represent standard deviation. (D) Influence matrix of the random network with low group strength taken as the representative case for Figure 6E (E) Representative cases of comparison of transition dynamics for Mesenchymal and hybrid steady states between WT and random network.

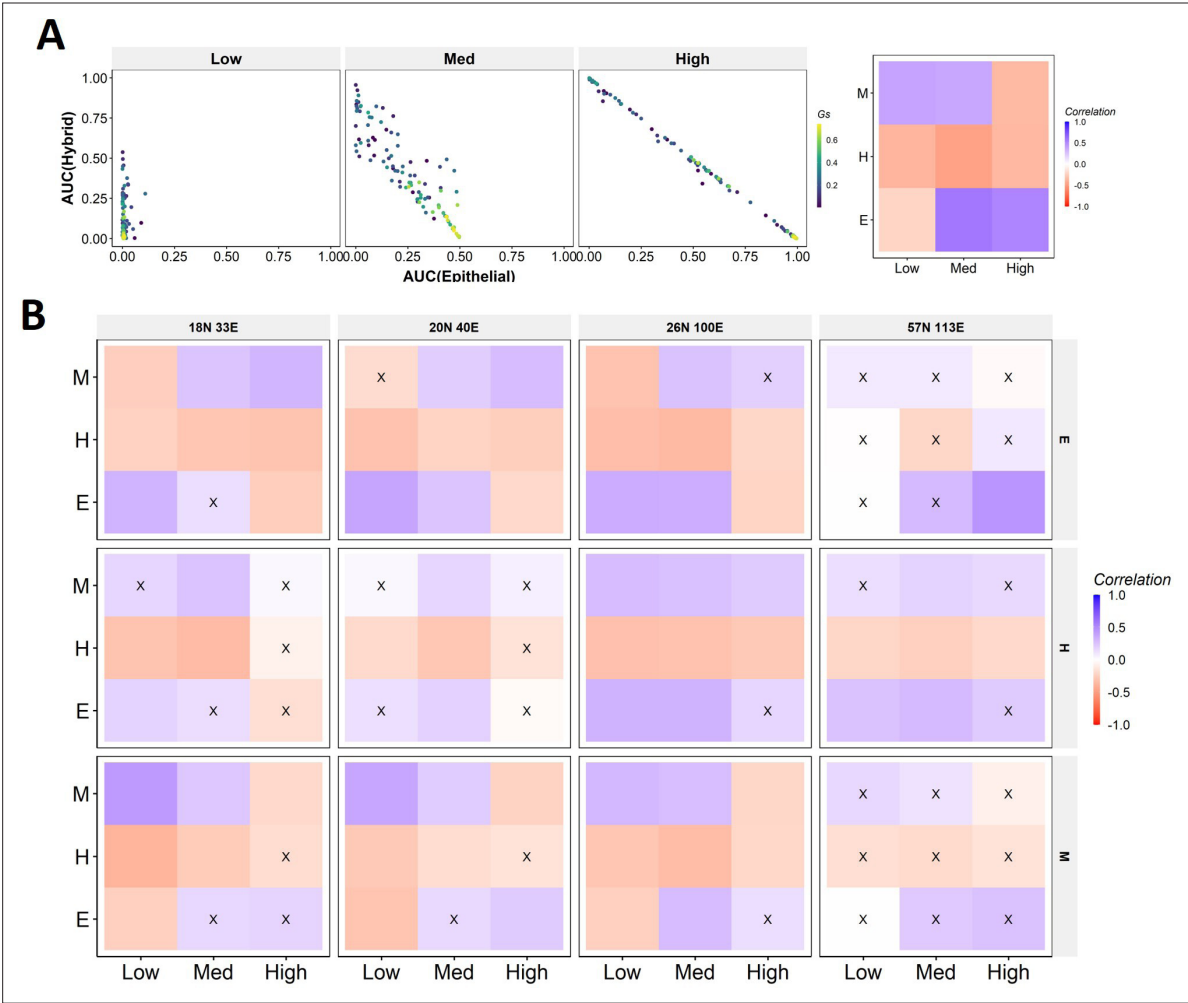


**Figure 6—figure supplement 2.** Coherence of calculated for the core nodes upon perturbing signal nodes in WT EMP networks. In each panel, x-axis represents individual steady states. y-axis represents the signals. The labels at the top (Init E, Init H, Init M) represents the phenotype of the steady states on x-axis. The labels to the right represent the class of core nodes for which coherence is calculated. Each cell represents the fraction of the corresponding core nodes retained in the steady state reached after the corresponding state is subjected to the corresponding signal perturbation.



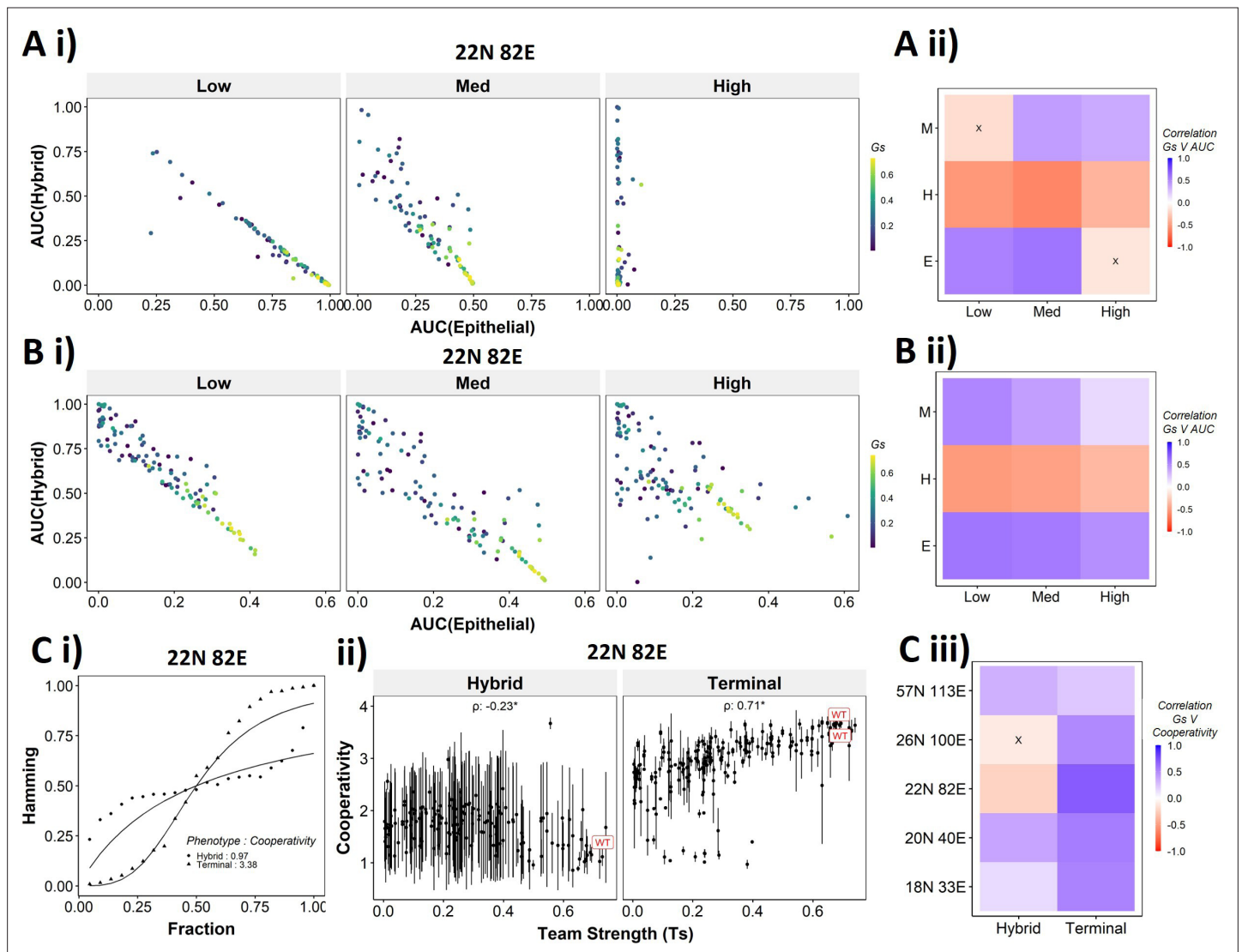


**Figure 7.** Distinction between the transition dynamics of hybrid and terminal phenotypes is lost as teams weaken. **(A)** (i) Scatter plot between mean AUC of Epithelial states and mean AUC of hybrid states when starting from epithelial phenotype. Each dot is a random network, colored by its team strength. (ii) Heatmap depicting the spearman correlation between team strength and AUC for the final phenotype (y-axis) and the regions in the sigmoidal plot (x-axis). **(B)** Same as F, but for Hybrid as the starting phenotypes. **(C)** (i) Depiction of cooperativity with a terminal and hybrid state of the WT EMP network 22 N 82E. (ii) team strength vs cooperativity for random and WT networks of size 22 N 82E. Each dot represents the mean cooperativity for one network. The bars show standard deviation. (iii) Correlation between team strength and cooperativity for random networks corresponding to WT EMP networks of different sizes.

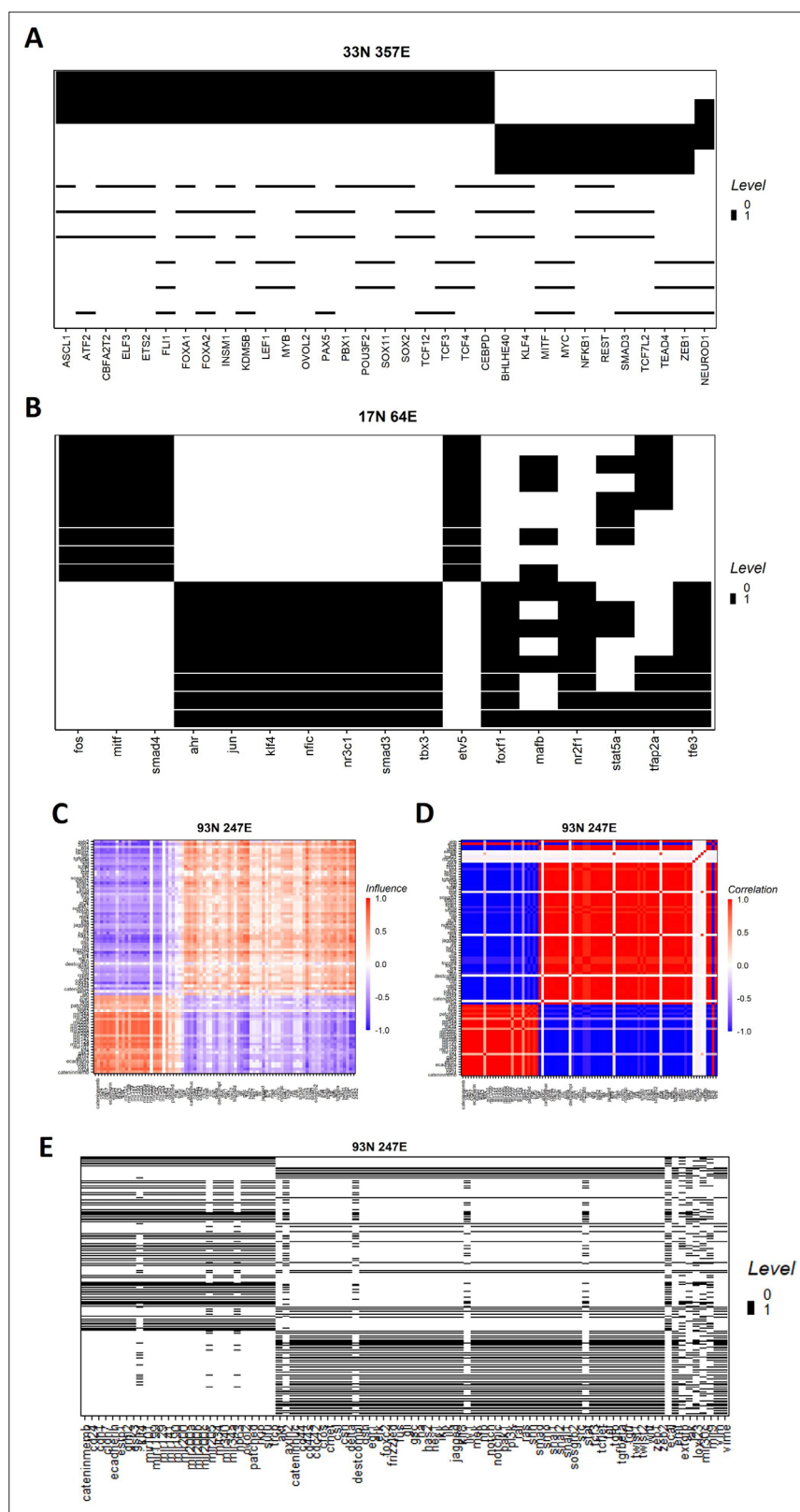


**Figure 7—figure supplement 1.** (A) Same as **Figure 7A** but for Mesenchymal phenotype as the beginning. (B) Heatmaps depicting the correlation between mean group strength and AUC for combinations of perturbation strengths and final phenotypes for all networks.

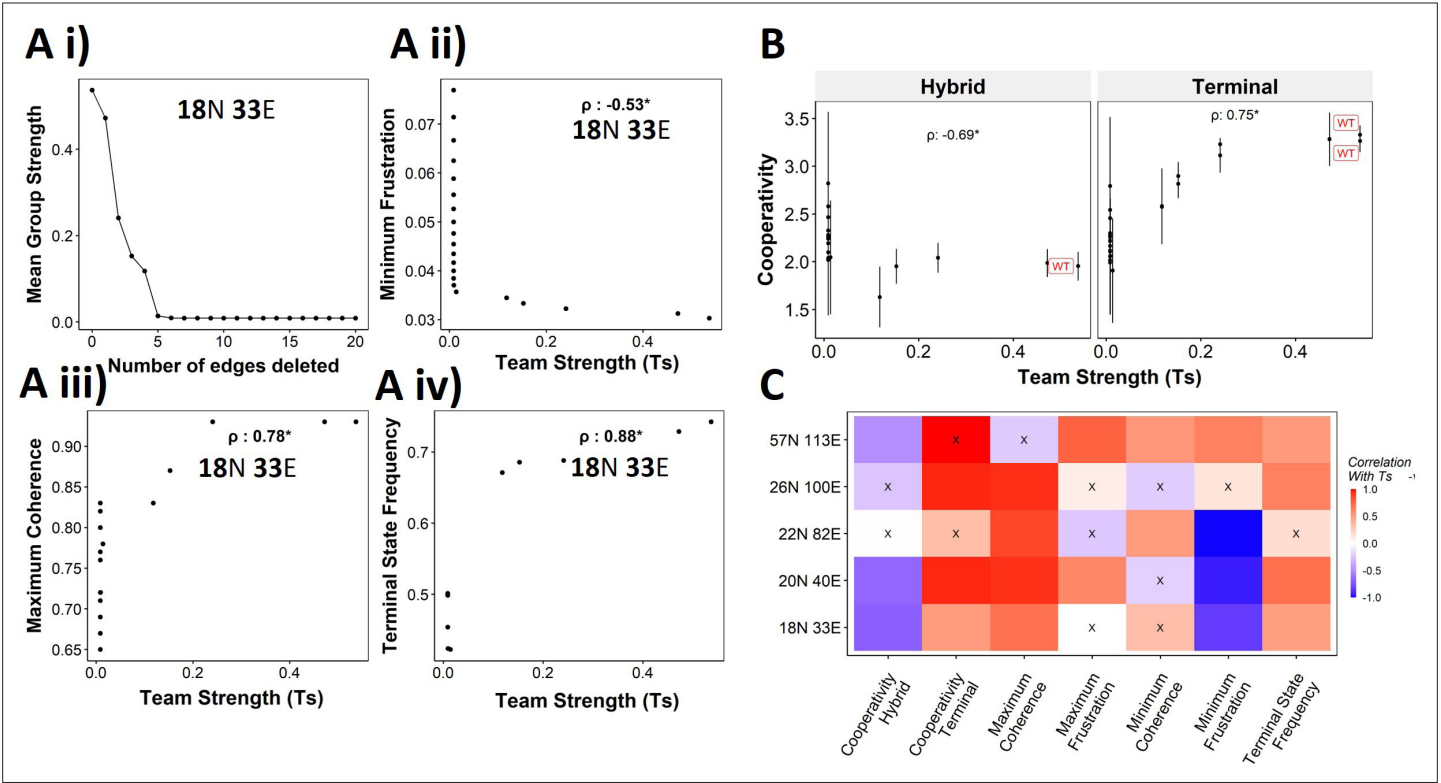


**Figure 8.** Reducing team strength leads to reduction in terminal phenotype stability. **(A)** (i) Lineplot to demonstrate the reduction of team strength with each edge perturbed. Change in (ii) Minimum Frustration, (iii) Maximum Coherence and (iv) Terminal state frequency with increase in team strength. **(B)** Mean cooperativity for the perturbed networks against the team strength. **(C)** Correlation between team strength and stability metrics for the perturbed networks (edge deleted one at a time sequentially as shown for 18 N 33E network in panel A) obtained from all five EMP networks.

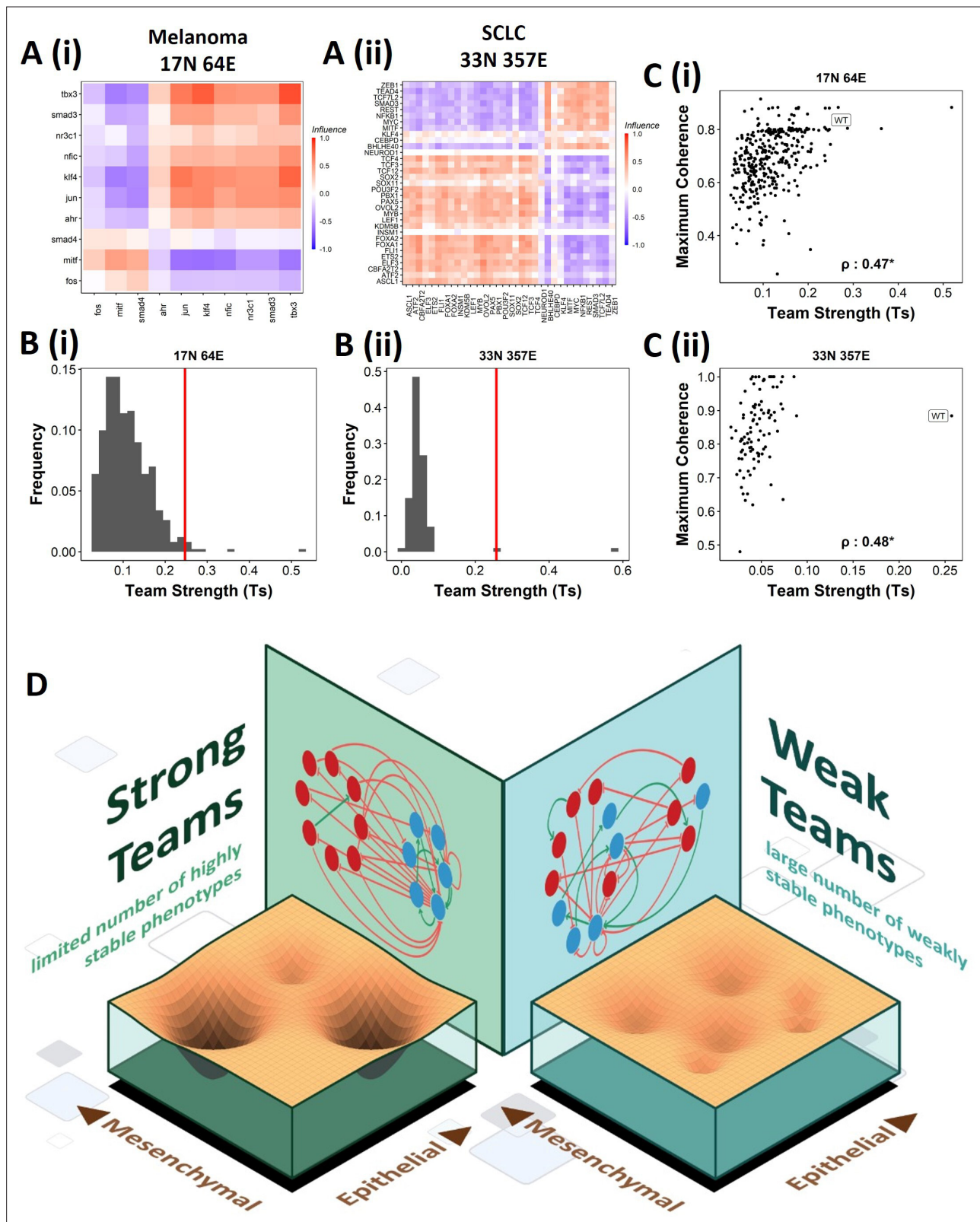


**Figure 9.** Effect of teams on phenotypic landscape in SCLC and melanoma. **(A)** Influence matrices of **(i)** Melanoma (17 N 64E) and **(ii)** SCLC (33 N 357E) networks, depicting the two team structure observed. **(B)** Comparison of team strength distributions obtained for random networks corresponding to **(i)** melanoma and **(ii)** SCLC, with the WT melanoma and SCLC team strengths labelled by red vertical line. **(C)** Scatterplots depicting the maximum coherence against the team strength of the random networks corresponding to **(i)** melanoma and **(ii)** SCLC. Spearman's correlation coefficient reported. \*:  $p < 0.05$  **(D)** Schematic showing the effect of team structure on the phenotypic stability landscape emergent from the network topology.

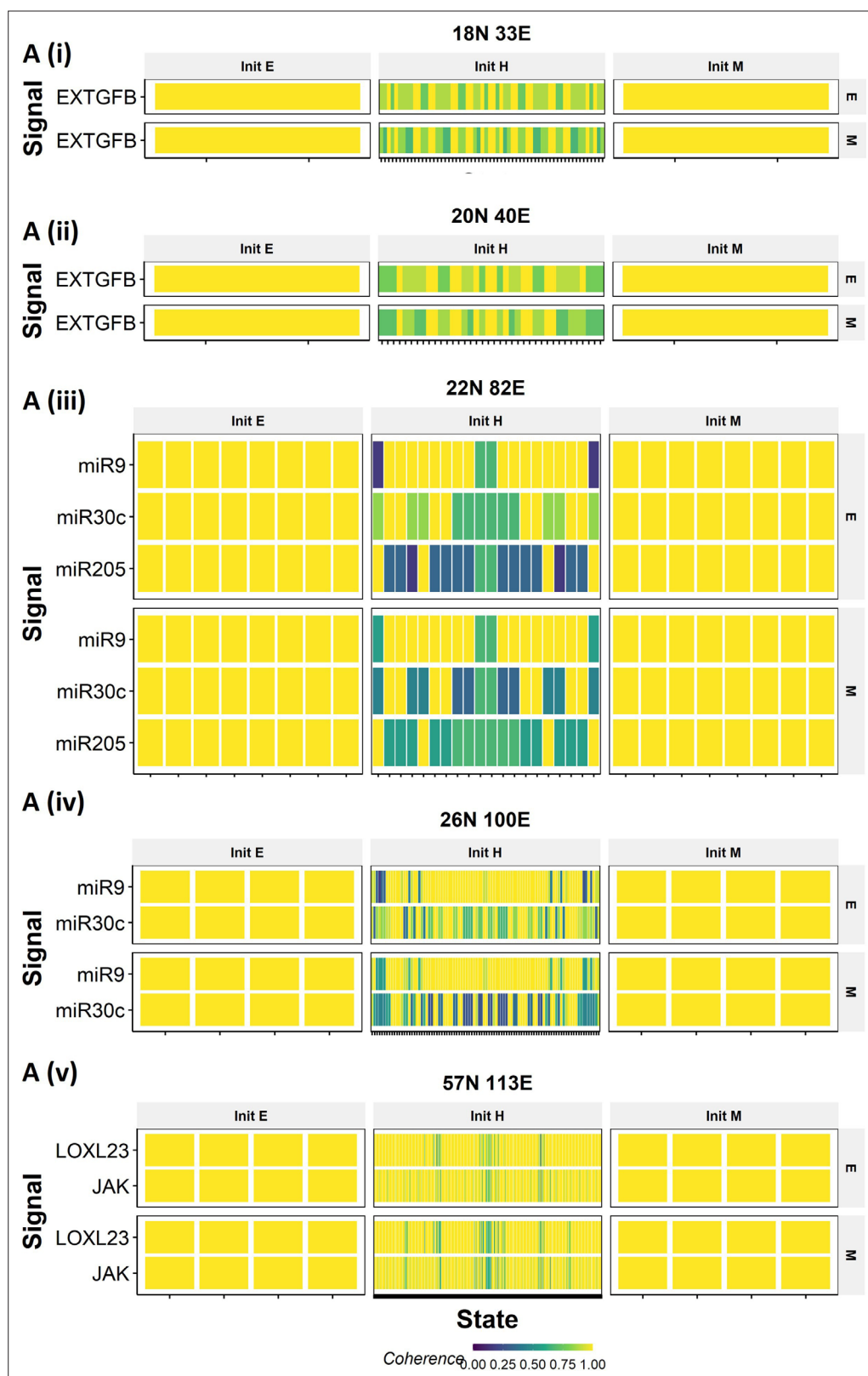


**Figure 9—figure supplement 1.** (A–B) Heatmaps showing the steady state composition and the corresponding SSF of (A) SCLC and (B) Melanoma GRNs. Each row represents a state and each column a node. The height of each row represents the SSF of that state. (C) Influence matrix of the combined EMP network. (D) Correlation matrix of the combined EMP network obtained from Boolean simulations. (E) Same as A–B, but for the combined EMP network.